Eur. Phys. J. Appl. Phys. (2012) 58: 11001
DOI: 10.1051/epjap/2012110295

THE EUROPEAN PHYSICAL JOURNAL
APPLIED PHYSICS

Regular Article

Focusing specular neutron reflectometry for small samples

J. Stahn[1,a], U. Filges[2], and T. Panzner[2]

[1] Laboratory for Neutron Scattering, Paul Scherrer Institut, 5232 Villigen PSI, Switzerland
[2] Laboratory for Developments and Methods, Paul Scherrer Institut, 5232 Villigen PSI, Switzerland

Received: 25 July 2011 / Received in final form: 18 November 2011 / Accepted: 1 March 2012
Published online: 23 March 2012 –

Abstract. In many areas of soft and hard matter research science, the amount of material to investigate is rather limited. Partly because the fabrication of larger samples is too expensive or not feasible, yet, partly because the interesting features depend on the size. The aim of this work is to develop a neutron reflectometer optimized for small samples and specular measurements. We present a new concept which is based on state-of-the-art neutron optical elements and which allows studies of samples 100 times smaller than with previous instrumentation. The concept is to use an elliptically focusing guide in the sample plane, and a converging beam geometry in the scattering plane. The latter allows for the simultaneous measurement of a wide angle-of-incidence range simultaneously. Here we report on the prototype setup and first measurements, where we reached a reduction of counting time by one order of magnitude. If a complete instrument is built based on the presented principle, another order of magnitude can be expected.

1 Introduction

Science and technology related to thin film heterostructures is a rapidly growing field. This reaches from biological membranes and their manipulation, via functional solid-state devices like magnetic recording media, to the investigation of fundamental physical processes like the interaction between magnetism and superconductivity. As the complexity of the films increases, their size is shrinking caused by the sheer price of the constituents (e.g., isotope-labeled exotic surface-active molecules), by the limits given by the film growth methods and by the technical applications, requiring uniform properties.

A widely used method to investigate the depth profiles of layered materials is X-ray or neutron reflectometry. The aim of this work is to present a neutron reflectometer optimized for small samples (i.e., surface area of 1–100 mm^2), and for specular measurements, where the design includes the flight path of the neutrons from the source to the detector [1]. The key component is an elliptic-shaped reflector. Its similarity to the elliptic light-to-shadow border on the moon gave the name for this concept: *Selene* is the titan goddess of the moon.

Neutron reflectometry is an established method to probe structural and magnetic depth profiles at surfaces. Especially the high sensitivity to magnetic induction and the possibility for isotope labeling make it a demanded technique [2]. A well-collimated neutron beam of defined wavelength λ is impinging on a surface at a grazing angle θ. The beam is partially reflected and refracted according to the density contrast at the surface and interfaces below. This results in interferences and the intensity of the specular reflected beam is thus a function of λ, θ, the layer thicknesses and densities.

In conventional reflectometers a well-collimated beam (defined by a distant slit and the sample size) hits the surface at an angle θ, is reflected by 2θ and finally detected. To scan the reflectivity R as a function of the momentum transfer $q_z = 4\pi \sin\theta/\lambda$, one can either vary θ or λ. The upper sketch in Figure 1 shows the layout of a typical time-of-flight neutron reflectometer, together with the scattering geometry at the sample. In this case λ is varied: a chopper before the sample creates a short polychromatic neutron pulse. The intensity reflected from the sample is measured as a function of the time-of-flight of the neutrons from the chopper to the detector, which is proportional to λ. The resolution is determined by $\Delta\theta$ (selected by the initial slit) and $\Delta\lambda$.

2 The concept

The measurement time in reflectometry scales with the illuminated sample area. For small samples (i.e., surface area below 1 cm^2) this means counting times of up to 12 h for one set of external parameters (such as temperature, fields and neutron spin state). It is thus too time consuming to screen several samples or external parameters like temperature or electric and magnetic fields at the sample with sufficient resolution. To overcome this problem at least for specular reflectometry, several concepts

[a] e-mail: jochen.stahn@psi.ch

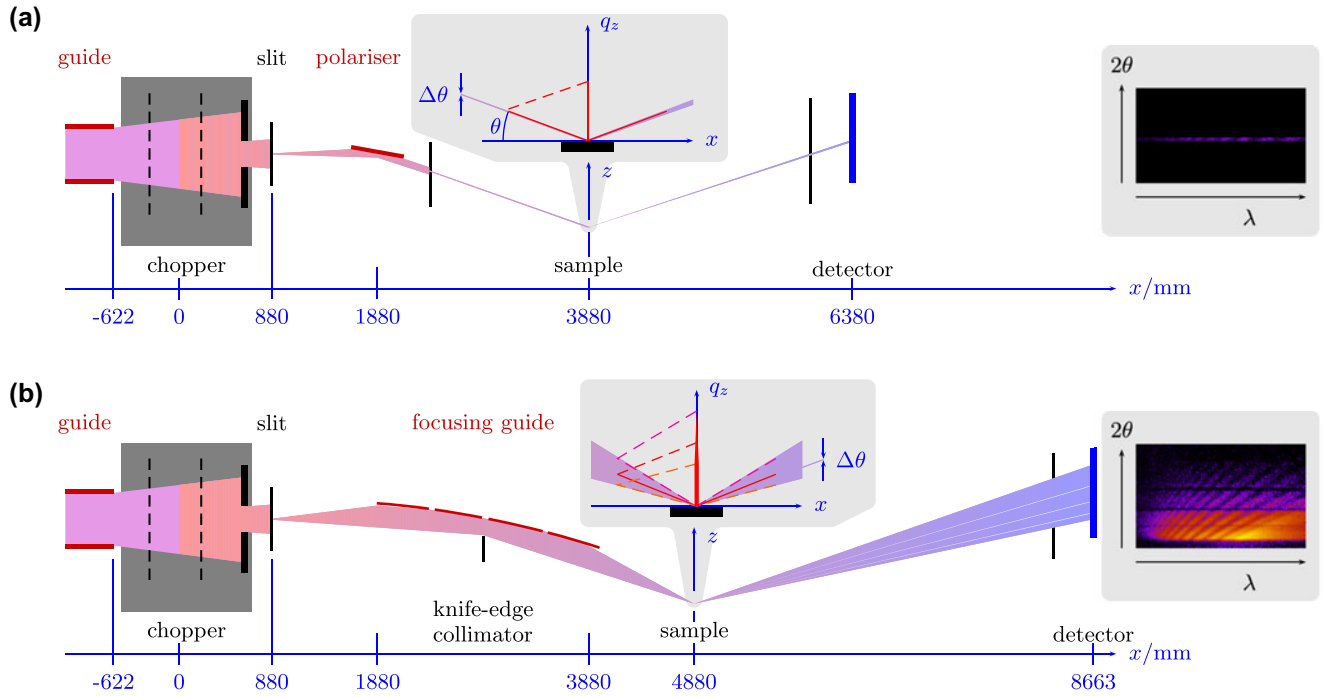

Fig. 1. Sketch of the neutron reflectometer Amor at PSI in the scattering plane. The polychromatic continuous neutron beam is delivered by a guide (from the left) and pulsed by a chopper. Figure (a) shows the *normal* time-of-flight operation mode with the beam being defined by slits before the sample. The inset displays the scattering geometry at the sample: a highly collimated beam is reflected off the surface. At one instant (i.e., wavelength) only one q_z is probed. Figure (b) shows the *Selene* setup: the divergent beam emerging from the first slit is focused onto the sample. At one instant a wide q_z range is probed simultaneously. θ is measured by the detector, and $\Delta\theta$ is given by its resolution. The maps on the right display the intensity over λ and θ, collected in both cases. The difference in the illuminated area corresponds to the gain one can obtain with the convergent beam geometry. (*Black*: diaphragms, absorber; *blue*: auxiliary lines; *dark red*: (coated) guide; *light red to blue*: neutron beam. The vertical axis is stretched by 10.)

have been developed over recent years. Some of them use a white continuous incident beam and perform an energy analysis on the reflected beam [3–5]. Another approach is to encode λ in θ in a broad, converging beam, focused onto the sample by an elliptically shaped neutron guide [4,6].

We modified the latter approach [1] and adapted it to time-of-flight instruments: the chopped beam with large $\Delta\theta$ is focused onto the sample. The reflected divergent beam is detected with a position-sensitive detector. The convergent beam is realized by a reflector of elliptic shape, which focuses the neutrons emerging from a small source in its first focal point to the sample in the second. Assuming a homogeneous intensity distribution vs. angle, the flux on the sample is proportional to $\Delta\theta$ (limited by the geometry and the reflectance of the reflector). The insets and the intensity maps in Figure 1 illustrate this.

One could also think of moving the sample closer to the (virtual) source to get the same divergence. That would simplify the setup and give at least the same flux on the sample. But there is a series of disadvantages: the full divergent beam overilluminates the sample area and thus leads to radiation and background problems. Polarization and wavelength filtering become more complicated. And in most cases the minimum distance to the source is of the order of 10 m, so that a guide is needed anyway.

Instead of the suggested elliptic guide, it is possible to use a parabolic-shaped one. In that case a parallel beam is converted into a convergent one. Its incoming divergence determines the spot size at the sample position. The definition of this spot then would require a collimator before the parabola. Assuming perfectly reflecting surfaces, and collimation without losses, both geometries give the same flux on the sample.

Reflecting bent surfaces are used for a long time as X-ray optics (e.g., Kirkpatrick-Baez [7] or Montel optics [8]). These concepts have been adapted for neutron optics, with a lower precision, but increased dimensions. Focusing elliptic neutron guides have been investigated and realized several times in the past [9–11] and they are the subject of several new concepts for neutron transport [12].

The focusing in the scattering plane intrinsic to this approach predestines it for small samples. Additional focusing in the sample plane increases the flux on small samples further. The increased divergence in this direction has a negligible effect on the in-plane reflectivity. The focusing in both directions is performed by the same device, a three-sided neutron guide with elliptical curvatures along the flight direction of the neutrons. Its cross-section is of rectangular shape.

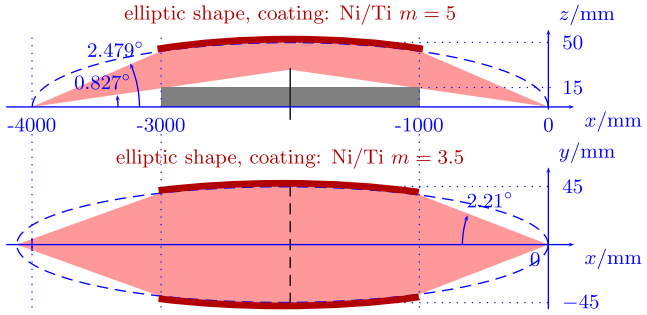

Fig. 2. Sketch of the elliptic guide with dimensions. The y and z scales are stretched by a factor of 10 relative to the x scale. *Top*: cut in the scattering plane (x-z-plane), *bottom*: cut in the sample plane (x-y-plane). The half-axis parameters are $a_{xz} = 2000$ mm, $b_{xz} = 50$ mm and $a_{xy} = 2025$ mm, $b_{xy} = 45$ mm.

3 The prototype

As a first step a prototype of an elliptic reflector was built and tested on Amor at SINQ, PSI. Amor is a versatile neutron reflectometer which allows for a wide range of setups [13]. The scattering plane is vertical so that liquid surfaces can be measured. Most components are positioned on an optical bench which allows to test pioneering setups like the prism approach by Cubitt [5] or the *Selene* concept.

For the presented setup, the end of the neutron guide is taken as a virtual source for cold neutrons (i.e., 2 Å $< \lambda <$ 30 Å). The guide limits the divergence for 4 Å neutrons to 1.6° in the scattering plane. The initial aperture defining the first focal point of the elliptic reflectometer is located behind the chopper. A 2 m long elliptically shaped reflector is mounted on the optical bench, the sample is moved to the second focal point. The reflected beam is detected with a position-sensitive detector, whose spatial resolution and distance to the sample determine the q_z-resolution (together with the λ-resolution). Amor is equipped with a ^{3}He wire detector with an active window size of 180 × 180 mm^2. It has a spatial resolution of ≈2 mm. To get the highest possible angular resolution for the reflected beam, the detector is positioned at the far end of the optical bench. A sketch of this setup is shown in the lower part of Figure 1.

The sample size in the scattering plane is given by the projection of the sample length normal to the incoming beam. This results in an effective height of less than 0.7 mm ($\theta < 4°$, sample length 10 mm). Initial aperture and sample position define the foci of the elliptic shape of the reflector. The spatial constraints on Amor lead to a focus-to-focus distance of 4000 mm. The actual length of the device is given by the maximum reflection angle for short wavelengths (defined to be 4 Å, which is at the flux maximum of the wavelength distribution at the instrument) and the divergence to be collected. Simulations and analytical calculations resulted in an optimum reflector length of 2000 mm, where the distances from its ends to both foci are 1000 mm. The complete reflector is coated with a Ni/Ti supermirror (SM) of $m = 5$ (m measures the critical angle of total external reflection of the SM relative to that of Ni). A sketch of the guide geometry is shown in Figure 2. The manufacturing of the glasses, the coating and the assembly were done by a commercial company (SwissNeutronics).

A knife-edge diaphragm (an absorbing blade forming an adjustable gap with the surface) is installed in the center of the elliptic guide to prevent the direct view, and to allow for small divergences if needed (e.g., for the sample alignment or for off-specular reflectometry).

The gain to be expected by the focusing in the scattering plane is illustrated in the right-hand side of Figure 1: for the conventional setup, only a small area of the detector is illuminated, where the *Selene* setup covers a large part of it.

A limitation for the *Selene* concept is that the off-specular scattering from the sample leads to a non-flat background, which might affect or even prohibit the extraction of $R(q_z)$ from the measured intensity map. But even in these cases it can be beneficial to use the *Selene* setup to screen the influence of external parameters, such as temperature, electric or magnetic fields or stress. The signal can be seen as a fingerprint: its changing with the external parameter marks a transition and tells us where to look more carefully with a narrow incident beam.

4 Experiments

For the first tests of the *Selene* setup on Amor, the following samples were used: a 100 nm thick Ni film on a glass substrate, a perovskite-type hetero-structure and a $m = 5$ SM on silicon. The latter has a reflectivity of the order of 1 up to $q_z = 0.11$ Å^{-1} and was used for normalization. The Ni films' reflectivity is characterized by total reflection up to $q_z = 0.022$ Å^{-1}, followed by beatings with exponentially falling intensity. The beatings are caused by the interference of the neutrons reflected at the air/Ni and the Ni/glass interfaces.

The chopper consists of two disks, 490 mm apart, each with two openings of 13.6°. It is operated in a way as to give $\Delta\lambda/\lambda = 6\%$ [14]. For these tests we used the low pulse frequency of 25 Hz (corresponding to 750 rpm) to reduce the overlap of subsequent pulses.

The diaphragm defining the pre-image had a height of 1 mm. Even with this rather small aperture one had to take care not to oversaturate the area detector, some 8 m away. This tells us that the bottleneck for a further optimization will be the performance of the neutron detector.

Figure 3 shows one measured intensity map and the corresponding result of a McStas simulation [16]. The fan-like pattern visible in the $I(\lambda, \theta)$ maps originates from the mentioned intensity beatings, expected for the Ni film. The lower map was calculated assuming a perfect guide and optimum alignment. A comparison with the experiment in the upper map indicates that these assumptions have not been fulfilled. Introducing some misalignment

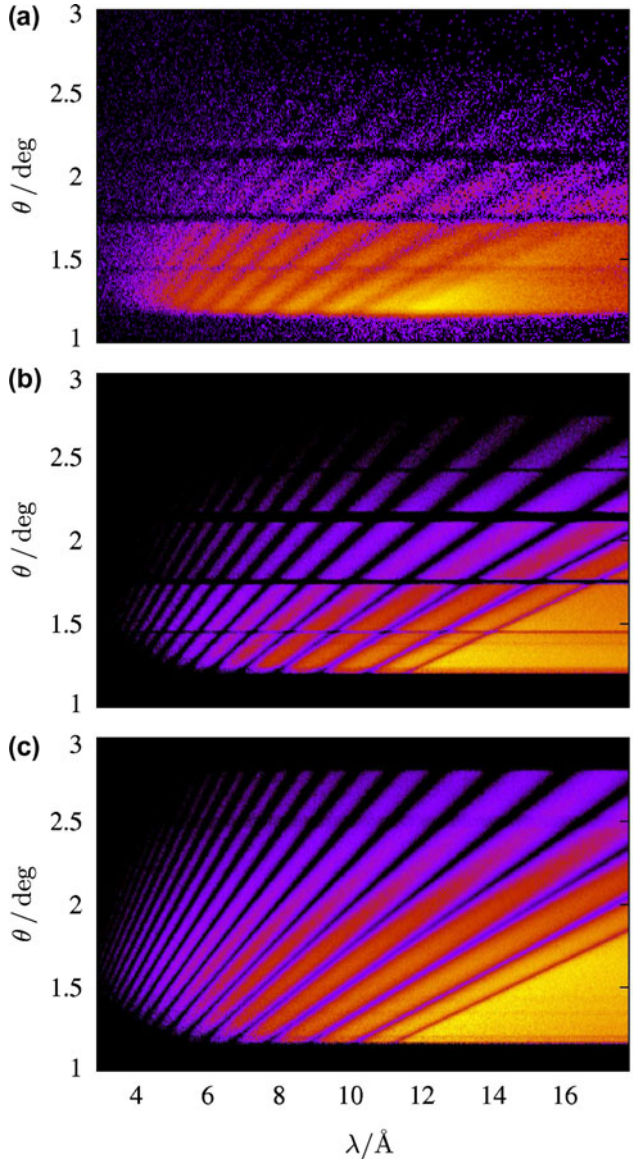

Fig. 3. Intensity maps as a function of λ and θ for a 1000 Å Ni film on glass. The intensity is given on $\log_{10}$ scale, where the color spectrum runs from black ($\log_{10} I = -3$) to yellow ($\log_{10} I = 0$). Map (a) is as measured and (b) compares to the simulated one. To reproduce the measured intensity distribution in the simulation, the guide segments had to be tilted up to 0.02° relative to each other and shifted in the μm range. Map (c) is also simulated, assuming a perfect alignment.

in the simulation allowed one to reproduce the measurements quite well (middle). The elliptic guide is assembled from four segments of 500 mm length, each (see Fig. 1). The regions close to the joints seem to have a shape deviating from the ellipse. Thus, the neutrons reflected there do not reach the sample. This is the origin of the prominent dark stripes.

For the analysis, the $I(\lambda, \theta)$ map is converted to a $I(q_z, \theta)$ map pixel by pixel. That is every line with constant θ is transformed into a $R(q_z)$ curve, where the SM

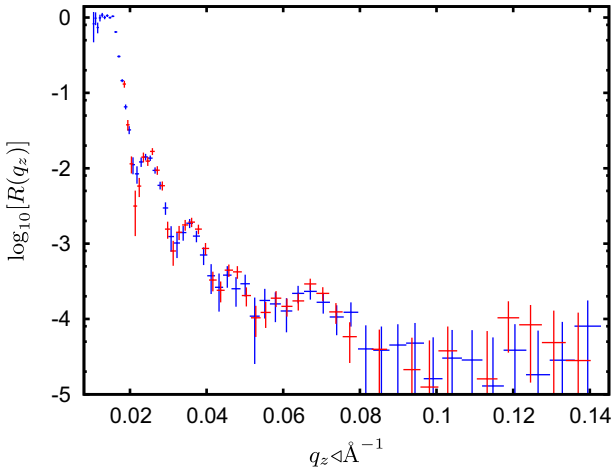

Fig. 4. $R(q_z)$ of the multilayer $Pr_{0.7}Ca_{0.3}MnO_3$ (70 Å)/[$LaAlO_3$ (30 Å)/$Pr_{0.7}Ca_{0.3}MnO_3$ (70 Å)]$_5$/$NdGaO_3$ measured with a conventional time-of-flight setup in 6.5 h (red), and using the focusing in the scattering plane in 45 min (blue). The sample size is 4 × 5 mm^2.

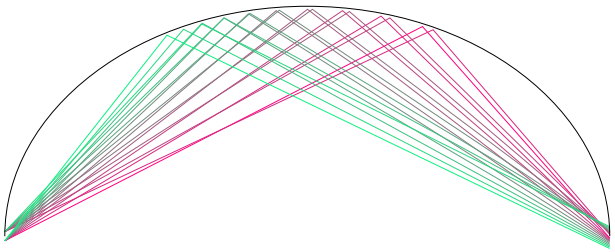

Fig. 5. Sketch to illustrate the effect of coma aberration. The pre-image consists of two point sources, located at $z = \pm 1$. The half-axis parameters used here are $a = 2000$, $b = 50$, the sketch is stretched by 30 normal to the long axis. The take-off angle α is encoded in the color of the beam. At the image position a clear separation of the colors can be seen. High α results in an almost parallel wide beam (green), while low α leads to a beam focused to the second focal point (red).

measurements were used for normalization. Subsequently all data points were merged into a new q_z grid. This summation is problematic if the q_z-resolution varies over the summation area. In this case the measurements have to be analyzed by comparison of the $R(q_z, \theta)$ maps, rather than using $R(q_z)$ curves.

The definition of a gain factor for the *Selene* setup relative to the conventional one is not straightforward because too many parameters (slits, distances, chopper frequency, etc.) are varied. We chose to compare the measurement times for a typical sample needed to obtain approximately the same resolution and statistics within the same q_z range. The instrument settings have been optimized for the respective setup. For the conventional mode that means twice the chopper speed, a shorter distance (see Fig. 1a) and an initial slit of 2 mm instead of 1 mm. Figure 4 shows $R(q_z)$ of a perovskite multilayer of 4 × 5 mm^2 area obtained this way, in comparison with the results of a conventional time-of-flight measurement

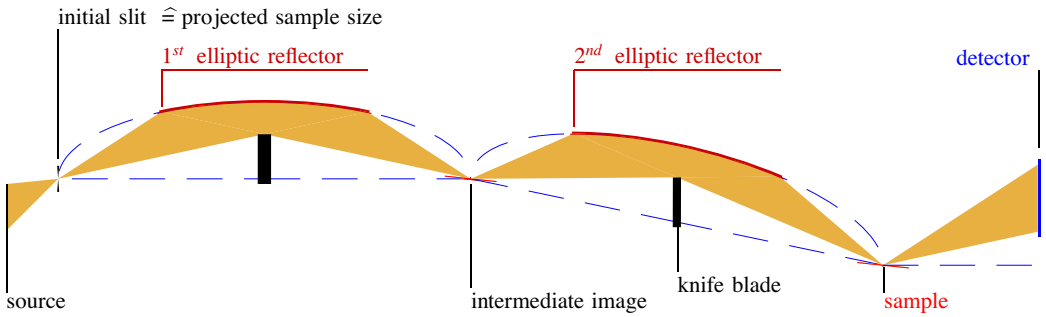

Fig. 6. Sketch of a full instrument using focusing elliptic guides in the scattering plane. The yellow area represents the neutron beam. At the position of the intermediate image a reflector allows for polarizing and adjusting the beam direction.

on the same sample. Both data were obtained with one sample orientation, only. A complete measurement includes up to four orientations. To be able to compare both measurement schemes this way, a variation of $\Delta q/q$ from 6.1% to 6.7% over the θ range has been accepted for the *Selene*-mode measurement (here $\Delta\lambda/\lambda = 6\%$ and $\Delta\theta_{\mathrm{detector}} = 0.03°$). This results in the lower resolution for small q_z which can be seen as a not so sharp first minimum. The difference in counting times to obtain these quantitatively equivalent curves gives us a gain factor of 7. For higher q_z the gain will be less, since there the incident beam is broader also in the conventional setup.

With a reflector of higher geometrical fidelity a gain factor of 10 could be reached on Amor. The main obstacle on this instrument is the divergence of the neutron beam reaching the initial slit. Example for $\lambda = 4$ Å, $I(\theta)$ has a plateau for $|\theta| < 0.5°$ and drops to almost 0 for $|\theta| > 0.8°$.

5 Full instrument

A principal problem with using elliptic reflectors for focusing is the coma aberration, inherent to this approach. Figure 5 displays this effect.

For typical elliptic reflectors and sample sizes, it turned out that due to the coma aberration the virtual source size has to be about three times the sample size. Then the complete sample is illuminated with the same divergence. As a consequence the beam spot at the sample is about 10 times the sample size, but the intensity drops fast outside the inner homogeneous region. One can estimate that about 30% of the beam hits the sample, the rest leads to illumination of the sample environment.

It is possible to correct for the coma aberration by dividing the reflector into two identical elliptic parts which have one focal point in common (see Fig. 6): the blurred intermediate image is converted back to a sharp image at the sample position. With an adjustable initial slit it is thus possible to just illuminate the sample with a homogeneous beam whose divergence is defined by the acceptance of the elliptic reflector.

This setup with two reflectors replaces the straight guide normally needed to bridge the distance (typically 10–40 m) between source and sample position. It allows to manipulate (polarization, λ-filtering) the beam at the position of the intermediate image where it is relatively small.

In the scattering plane the instrument then has a layout as sketched in Figure 6. As early as possible after the source an initial aperture of the maximum size of the beam spot at the sample is installed. That is about 1×10 mm^2 instead of the usual guide cross-section of 2000–3000 mm^2. This means that two orders of magnitude less neutrons enter the guide, and thus radiation problems are much reduced. This pre-image is mapped to a (blurred) intermediate image of about 3×30 mm^2 by an elliptic reflector. That can be manipulated by a small chopper, a monochromator, a polarizer or the like. An identical second reflector maps the manipulated intermediate image to the sample position.

6 Conclusion

We proved with our setup that the *Selene* concept leads to a time reduction for specular measurements of one order of magnitude. This value can be increased by optimizing the guide and using in-plane focusing. Both items are currently under development.

We will repeat the measurements also for more demanding samples and for higher q_z ranges to check the limits of the method. That is the influence of off-specular scattering and the dynamic range is reachable.

With the presented data we fortify our recommendation to use this concept for new reflectometry beam lines: it allows one to start with a tiny aperture, close to the cold source and thus reduces radiation and shielding problems by orders of magnitude. By using two elliptic guides in series aberration can be avoided, and it is possible to manipulate the beam at the joining focal point, e.g., by a polarizer or a chopper. With the aperture reducing the divergence one has the full functionality of the conventional time-of-flight or angle dispersive setups, allowing for off-specular reflectometry.

For ideas and discussion, we thank F. Ott, B. Cubitt, P. Böni, U. Stuhr, C. Schanzer, M. Zhernenkov, H. Wacklin, C. Niedermayer and many others. Special thanks to C. Aruta and

F. Miletto for kindly providing the PCMO/LAO multilayer sample for these tests.

This work is based on experiments performed on Amor at the Swiss spallation neutron source SINQ, Paul Scherrer Institute, Villigen, Switzerland. It has been supported – by the European Commission under the 7th Framework Program through the *Research Infrastructures* action of the *Capacities* Program, Contract No. CP-CSA_INFRA-2008-1.1.1. Number 226507-NMI3 – by the Swiss National Science Foundation through the *NCCR – Economic stimulus package: Neutron optical devices for small samples*; and – by SwissNeutronics.

References

1. J. Stahn et al., Nucl. Instrum. Methods Phys. Res. A **634** S12 (2011)
2. J. Daillant, A. Gibaud, in *X-Ray and Neutron Reflectivity: Principles and Applications*, Lecture Notes in Physics 58, (Springer-Verlag, Berlin, Heidelberg, New York, 1999)
3. F. Ott, Nucl. Instrum. Methods Phys. Res. A **584**, 401 (2008)
4. F. Ott, A. Menelle, Eur. Phys. J. Special Topics **167**, 93 (2009)
5. R. Cubitt, Nucl. Instrum. Methods Phys. Res. A **558**, 547 (2006)
6. F. Ott, A. Menelle, Nucl. Instrum. Methods Phys. Res. A **586**, 23 (2008)
7. P. Kirkpatrick, A.V. Baez, J. Opt. Soc. Am. **38**, 766 (1948)
8. M. Montel, *X-Ray Microscopy and Microradiography* (Academic Press, New York, 1957), p. 177
9. U. Stuhr, M. Grosse, W. Wagner, J. Mater. Sci. Eng. A **437**, 134 (2006)
10. S. Mühlbauer et al., Nucl. Instrum. Methods Phys. Res. A **586**, 77 (2008)
11. S. Mühlbauer et al., Physica B **385–386**, 1247 (2006)
12. P. Böni, Nucl. Instrum. Methods Phys. Res. A **586**, 1 (2007)
13. M. Gupta et al., Pramana J. Phys. **63**, 57 (2004)
14. A.A. van Well, Physica B: Condens. Matter **180–181**, 959 (1992)
15. J. Stahn, Physica B: Condens. Matter **345**, 243 (2004)
16. K. Lefmann, K. Nielsen, Neutron News **10**, 20 (1999)